CHEMISTRY

TiO_2 metasurfaces: From visible planar photonics to photochemistry

Yunkai Wu[1]*, Wenhong Yang[1]*, Yubin Fan[1], Qinghai Song[1,2†], Shumin Xiao[1,2†]

TiO_2 metasurfaces have been intensively studied in the past few years. To date, the TiO_2 metadevices only used their high reflective index (*n*). The controllable light extinction coefficient (*k*) of TiO_2 has not been exploited yet. Here, we converted TiO_2 metasurfaces to black TiO_2 metasurfaces and explored their new opportunities in photochemistry. A complementary metal oxide semiconductor (CMOS)–compatible technique has been developed to reversibly and precisely control the absorption of TiO_2 metasurfaces without spoiling their internal nanostructures. Consequently, two types of black TiO_2 metasurfaces were realized for photochemical experiments. The metasurface with an ultrawide absorption band can substantially enhance the white light absorption and accelerate the solar-based photochemistry process by a factor of 18.7. The other metasurface with an absorption band of <20 nm only responded to the resonant wavelengths, making the photochemistry process capable of being monitored in real time. In addition, the reversible switch between normal and black states makes TiO_2 metasurfaces suitable for dynamic metadevices as well.

INTRODUCTION

A CMOS-compatible technique has been developed to switch between TiO_2 and black TiO_2 without spoiling their internal nanostructures, successfully extending the practical applications of TiO_2 metasurfaces from static planar visible photonics to dynamic metadevices and photochemistry. The field of metasurfaces has been one of the important driving forces for the advancement of nanophotonics (*1*–*4*). By constructing nanoparticles with subwavelength spaces, the planar metasurface enables many new physics and phenomena, providing a unique capability to fully control the incoming light and realize planar photonic circuits. In the past decade, while various metadevices have been demonstrated with silicon and plasmonic materials, their performances are limited by the material losses in the visible spectrum (*1*–*10*). Recently, TiO_2 has shown a series of intrinsic advantages for visible metasurfaces. It is transparent in the entire visible spectrum, and its refractive index is high enough to support Mie magnetic (electric) dipole resonances in a single nanoparticle. In 2016, Khorasaninejad *et al.* experimentally demonstrated the first TiO_2 metalens with efficiency above 70% in the entire visible range (*11*). Soon after, TiO_2 metasurface–based holograms, color nanoprinting, and spin orbital conversion were reported by different groups (*12*–*15*). Very recently, the chromatism of TiO_2 metasurfaces has also been successfully corrected (*16*–*19*). To date, the physics of TiO_2 metasurfaces are almost complete, and the research attention gradually switches to practical applications. However, despite the above progresses and the recent advances on synchrotron radiation (*20*) and optical coherence tomography (*21*), research on TiO_2 metasurfaces is mostly restricted in static photonic devices.

Titanium dioxide can absorb light with energy larger than its bandgap and then generate excited electrons and holes in the conduction and valence bands (*22*). Such excited charges have the ability of migrating individually to the surfaces of nanoparticles and performing photocatalytic reactions. Consequently, the combination with photocatalysis can be an emerging opportunity for TiO_2 metasurfaces. However, there is a barrier between these two research areas. The TiO_2 metasurfaces usually work in visible spectrum, whereas TiO_2 catalysts absorb ultraviolet (UV) light. While the conversion of TiO_2 to black TiO_2, pioneered by Chen *et al.* in 2011 (*23*), can reduce the bandgap to ~1 eV and increase the absorption in visible to near-infrared regions, the typical conversion techniques are strongly dependent on high pressure/high temperature (*23*–*26*), which spoil the internal nanostructures and thus are incompatible with TiO_2 metasurfaces.

Here, we develop a CMOS-compatible technique to produce black TiO_2 metasurfaces and explore their new opportunities in photochemistry. Basically, the TiO_2 film was deposited onto an Indium tin oxide (ITO)–coated glass substrate with the electron-beam (E-beam) evaporation technique (see Materials and Methods). The structural characterizations show that the deposited TiO_2 is an amorphous film with surface roughness <2 nm (fig. S1A). Then, the deposited TiO_2 film was placed into an inductively coupled plasma (ICP) etcher (Oxford PlasmaPro 100 Cobra) and implanted with H^+ ions for 4 min (see schematic picture in Fig. 1A and details in Materials and Methods). After the ion implantation, the color of the TiO_2 film changed from transparent to dark brown (see inset in Fig. 1A). The corresponding absorption spectra before and after H^+ ion implantation are plotted as solid and dashed lines in Fig. 1B. The absorption is significantly increased over the full visible spectrum, although a dip appeared at 400 to 480 nm. The corresponding x-ray photoelectron spectroscopy measurements show that Ti^{3+} species and oxygen vacancies are produced during the ion implantation (fig. S2, C and D) (*27*, *28*). All these observations are consistent with previous reports (*23*–*26*) and confirm the formation of black TiO_2 (fig. S2). The transition process between TiO_2 and black TiO_2 was reversible. By implanting O^- ions into the black TiO_2 film with ICP, the oxygen vacancies were recovered by oxygen ions. Then, both the absorption spectrum (dash-dotted line in Fig. 1B) and the color were restored.

Compared with previous techniques (*23*–*26*), the reversible transition process with ICP has several intrinsic advantages. More than the black and white, a series of interstates of the TiO_2 film can be

[1]State Key Laboratory on Tunable Laser Technology, Ministry of Industry and Information Technology Key Lab of Micro-Nano Optoelectronic Information System, Shenzhen Graduate School, Harbin Institute of Technology, Shenzhen 518055, P. R. China. [2]Collaborative Innovation Center of Extreme Optics, Shanxi University, Taiyuan 030006, P. R. China.
*These authors contributed equally to this work.
†Corresponding author. Email: shumin.xiao@hit.edu.cn (S.X.); qinghai.song@hit.edu.cn (Q.S.)

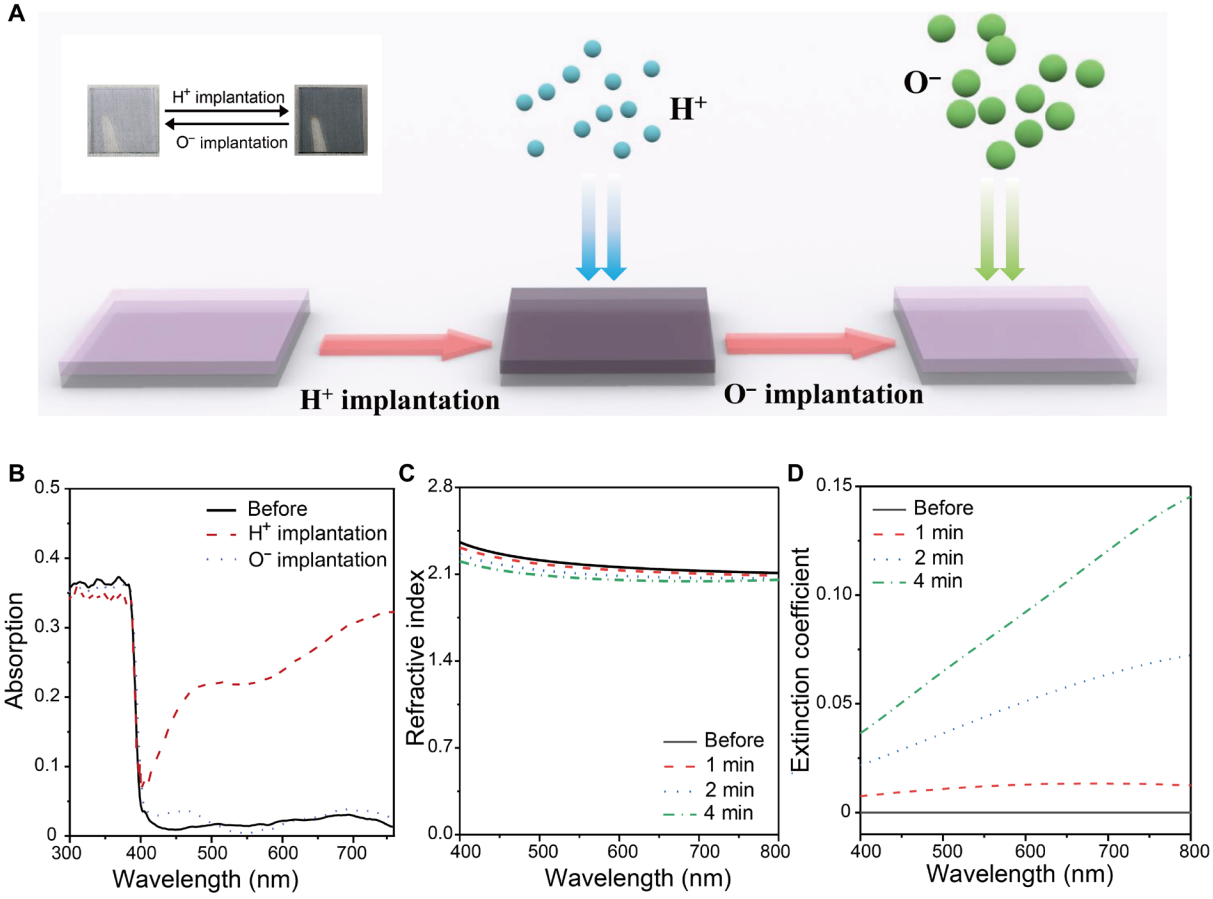

Fig. 1. The properties of the black TiO_2 film. (**A**) Schematic picture for the transition process between conventional TiO_2 and black TiO_2. The insets show the corresponding microscope images of TiO_2 films. (**B**) Dashed, solid, and dash-dotted lines are the absorption spectra of TiO_2 film before and after 4-min H^+ ion implantation and the recovered TiO_2 film. (**C**) and (**D**) show the refractive index *n* and light extinction coefficient *k* as a function of ion implantation time.

generated by controlling the ion implanting time. Figure 1 (C and D) shows the experimentally measured *n* and *k* as a function of ion implanting conditions. With the increase of implanting time from 0 to 4 min, the refractive index is kept around its initial value ($n > 2.1$), whereas the light extinction coefficient increases from 0 to 0.15 at 800 nm. The high-resolution scanning electron microscope (SEM) images show that the nanostructures of TiO_2 are well preserved during the transition processes (figs. S1 and S3, B and C). In this sense, the preserved refractive index and nanostructure can ensure the designed eigenmode of each TiO_2 nanoblock, whereas the tunable *k* value is able to precisely tailor the absorption and intensity of the incident light.

To further confirm adaptability, we fabricated TiO_2 metasurfaces and measured their reflection spectra before and after conversion to exclude the global changes (*29*) (see Materials and Methods and fig. S3). The TiO_2 metasurfaces were composed of periodic TiO_2 nanoblocks with lattice size *l* and side width *w* (see Fig. 2A). The cross section of each TiO_2 nanoparticle in the vertical direction was a trapezoid with a thickness of 200 nm and an angle of 72° (see fig. S3). The coupling between the magnetic (electric) dipole resonances and the reflection of the periodic structure can greatly enhance the reflectance and narrow the full width at half maximum (FWHM) (*30*). One example with $l = 400$ nm and $w = 330$ nm is illustrated in the bottom panel of Fig. 2B. A resonant peak with reflectance ~70% and FWHM ~20 nm can be seen at 637 nm. The reflectance at other wavelengths is close to zero. As a result, a distinct red color was obtained under a bright-field microscope (see inset). With the decrease of lattice size, the reflection peak gradually shifted from 637 to 607, 590, 561, 529, 513, and 481 nm in Fig. 2B. The recorded bright-field colors change from red to green and lastly to blue. In our experiment, 15 TiO_2 metasurfaces with different sizes have been investigated (see fig. S7B). Their reflection spectra were recorded and summarized as white dots in a International Commission on Illumination (CIE) 1931 color map, which covered a large area and indicated the potential of the TiO_2 metasurface in color nanoprinting.

Then, the TiO_2 metasurfaces were converted to black TiO_2 metasurfaces via ion implantation. Taking three metasurfaces with red, green, and blue colors as examples, we have carefully studied their performances with the ion implanting time. The experimental results are shown in Fig. 3A. The initial reflectance of three metasurfaces was around 70% at 627 nm, 60% at 550 nm, and 50% at 472 nm. After 1-min H^+ ion implantation, while the reflection peaks were kept at their original wavelengths, the intensities were greatly reduced to ~30%, and the corresponding structural colors became pale. By increasing the H^+ ion implantation time to 4 min, the intensities of reflection peaks further reduced to <10%, and the structural colors were all dark. To exclude the structural changes, we have converted the black TiO_2 metasurfaces back to TiO_2 metasurfaces

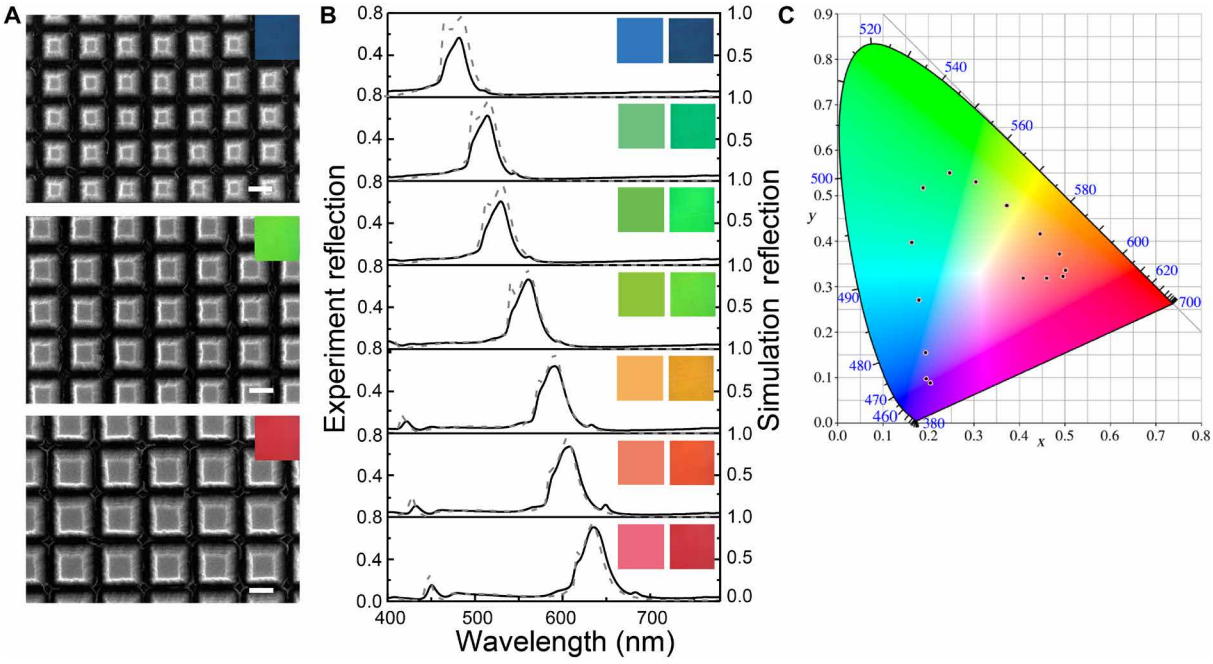

Fig. 2. The conventional TiO_2 metasurfaces. (**A**) Top-view SEM images of TiO_2 metasurfaces. Scale bars, 200 nm. The insets show the corresponding structural colors under a bright-field microscope. (**B**) Measured (solid lines) and numerically calculated (dashed lines) reflection spectra. From bottom to top, the lattice size decreases from 400 to 380, 370, 350, 330, 320, and 300 nm. The gap is kept at $w = 70$ nm. The insets are the recorded (left) and calculated (right) structural colors. (**C**) Corresponding structural colors of 15 metasurfaces in the CIE 1931 map.

with 5-min O^- ion implantation. As shown in the bottom panel of Fig. 3A, all the reflection peaks and the distinct colors were recovered. Figure 3B summarizes the reflectance of three metasurfaces as a function of transition rounds. No obvious reductions in reflectance were observed even after 20 TiO_2–black TiO_2–TiO_2 transition rounds (fig. S7A). Associated with the SEM images, the reflection spectra confirmed that our ion implantation process did not damage the TiO_2 nanostructures. Therefore, the CMOS-compatible technique has the capability of breaking the barrier and extending the applications of TiO_2 metasurfaces to photochemistry.

The color erasure with transition to black TiO_2 was quite generic. Figure 3C summarizes the recorded colors of 15 metasurfaces before and after H^+ ion implantation. We can see that the designed rainbow colors were all erased, and only the dark backgrounds were left (Fig. 3C). The corresponding CIE 1931 map in Fig. 3D shows that all the colors contracted significantly. This kind of post-synthetic control of structural color can produce by-products for TiO_2 metasurfaces. Figure 3E shows the top-view SEM image of the metasurface. Two types of TiO_2 metasurfaces with l = 300 nm and l = 290 nm were selected to construct the information and background, respectively. When the metasurface was illuminated with a white light source, a yellow "color" appeared in a green background (Fig. 3F). Once the metasurface was implanted with H^+ ions for 4 min, all the distinct colors disappeared, and the encoded information was fully concealed in Fig. 3G. Owing to the similar structural sizes between the information and background, the encoded information was even hard to resolve in the SEM image without the guiding lines (fig. S8), making the optical encryption more difficult to crack. The optical encryption process has also been concealed and recovered for many rounds, like their plasmonic counterparts (*31*, *32*). This technique has a series of intrinsic advantages for optical encryption. The brightness can be precisely controlled at will. It is independent of the cumbersome external instruments and compatible to modern CMOS technology, which are key factors for commercial applications.

Compared with the by-products as dynamic photonic devices, it is more interesting to explore new opportunities of black TiO_2 metasurfaces in photochemistry (*33*, *34*). In the case of photochemistry, one of the key experiments is solar-driven photocatalysis. Here, we take the photoreduction of Ag nano- and microparticles as an example to illustrate the impacts of black TiO_2 (*35*) because the photoreduction of Ag nanoparticles is visual and the reaction intensity can be directly evaluated by calculating the mean particle sizes of the generated Ag nanoparticles. This photoreduction process of Ag nanoparticles on top of the metasurface also provides a possibility to fabricate composite nanostructures with various excellent optical properties (*36*). While a conventional black TiO_2 film can absorb visible light and reduce Ag particles with solar light (see Fig. 4A), the reaction speed is strongly limited by the absorption dip around 400 to 480 nm (see Fig. 1B) and the small contact area between photocatalysis and solution. These limitations can be simply overcome by patterning the TiO_2 film into a TiO_2 metasurface. The metasurface had lattice size l = 285 nm and a reflection peak with reflectance >50% at 450 nm (see Fig. 4B). Figure 4C shows the corresponding absorption spectrum of the black TiO_2 metasurface. In contrast to a thin film, the resonance of light around 450 nm could greatly enhance the absorption time, and thus, the absorption gap was filled. The improved absorptance at shorter wavelengths, associated with the large contact area of nanostructures, makes the black TiO_2 metasurface suitable for photochemical experiments.

We then demonstrated the influences of the black TiO_2 metasurface on photochemistry by immersing the black TiO_2 metasurface in $AgNO_3$ solution (0.25 M) and illuminating it with a white light lamp

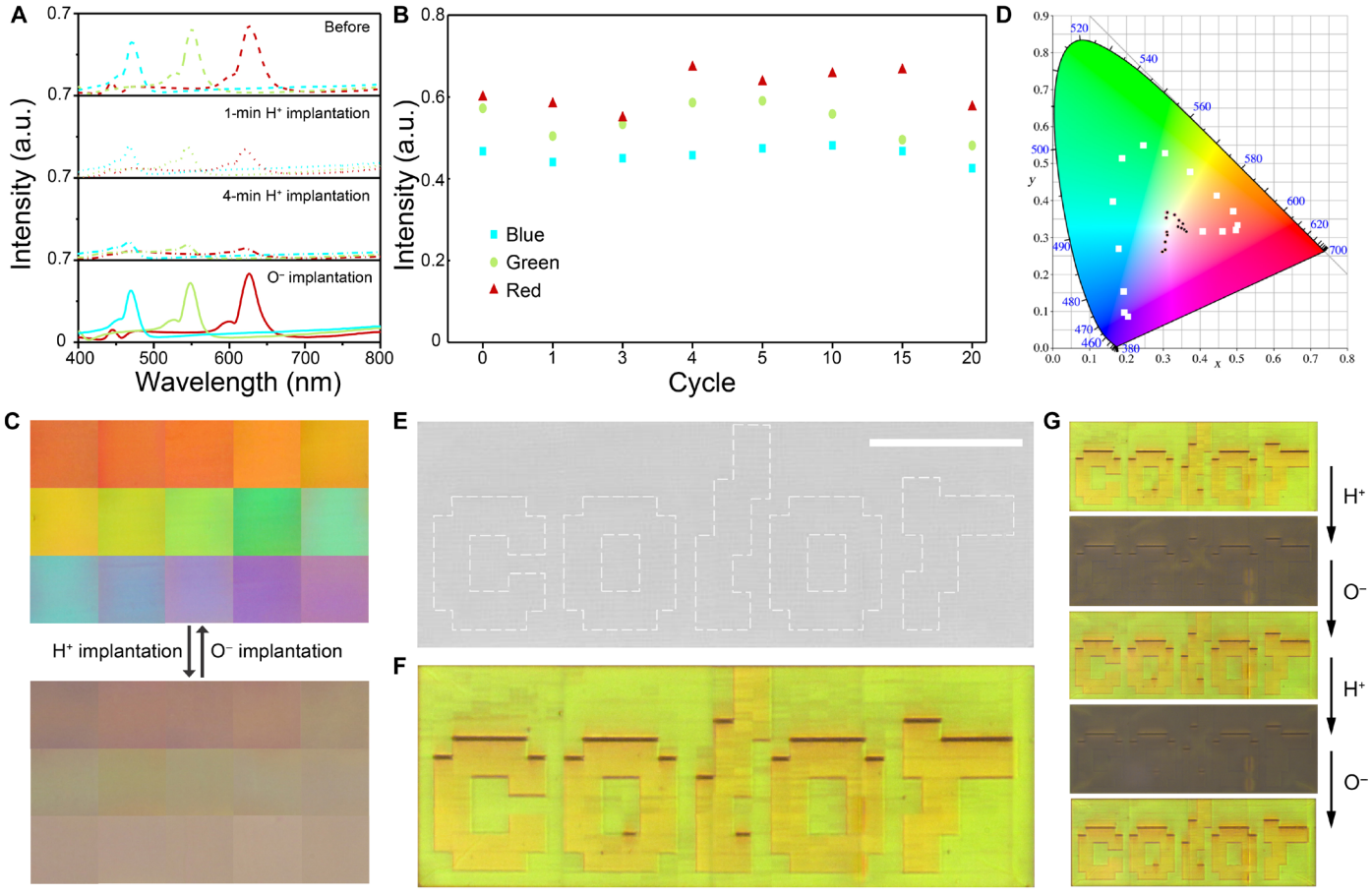

Fig. 3. The erased structural colors of TiO_2 metasurfaces and optical encryption. (**A**) Reflection spectra of three TiO_2 metasurfaces with $l = 330$ nm, $l = 280$ nm, and $l = 230$ nm before implantation (dashed lines), after 1-min ion implantation (dotted lines), after 4-min ion implantation (dash-dotted lines), and lastly recovered with O^- implantation (solid lines). The insets were the corresponding structural colors under a bright-field microscope. (**B**) Reversible transition of the TiO_2 metasurfaces as a function of transition rounds. No obvious degradation can be observed. (**C**) Color transitions of total 15 TiO_2 metasurfaces with different lattice sizes. (**D**) Corresponding transitions in the International Commission on Illumination (CIE) 1931 map. (**E**) Top-view SEM image of the encoded information and the background. The information "COLOR" is guided with dashed lines. Scale bar, 10 μm. (**F**) Displayed color image under a bright-field microscope. (**G**) Reversible color switch before and after H^+ ion implantation and O^- implantation for several rounds. a.u., arbitrary units.

(0.1 mJ/cm^2, the UV light has been filtered out) (fig. S9). Here, the immersing time was fixed at 60 s, and the illuminating time changed from 0 to 60 s. The morphological changes of black TiO_2 metasurfaces were characterized by SEM. Additional particles appeared after immersing the metasurface in $AgNO_3$ solution. With the increase of illumination time, the sizes of the nanoparticles also increased (Fig. 4D). The corresponding transmission electron microscope measurements confirmed that these new generated nanoparticles were Ag nanoparticles (fig. S10C). By measuring all the particles in a 6-μm^2 area on the metasurface, the mean sizes of Ag particles have been statistically analyzed and plotted in Fig. 4E. With the increase of illumination time from 0 to 20, 40, and 60 s, the mean sizes of Ag nanoparticles increased linearly from 0.09 to 0.53, 0.78, and 1.12 μm (see fig. S11A and examples in fig. S10). The nanoparticle with 0-s illumination is caused by the spontaneous reduction that relates to oxygen vacancies at the surfaces (*37*).

To confirm the effects of the black TiO_2 metasurface, two control experiments with a regular TiO_2 metasurface and a black TiO_2 film have also been performed under the same conditions. By immersing the regular TiO_2 metasurface into $AgNO_3$ solution and illuminating with white light, the displayed colors were well kept, and no additional nanoparticles have been generated (fig. S10D). The black TiO_2 film indeed produced some additional Ag nanoparticles. However, the particle sizes were much smaller than the ones on black TiO_2 metasurfaces (fig. S10F). The two control experiments have also been plotted as a triangle line and a dot line in Fig. 4E. We can see that the speed of photoreduction on the black TiO_2 metasurface was ~18.7 times faster than the value on the black TiO_2 film. Then, we confirmed that the black TiO_2 metasurfaces can improve the photochemical processes and are more suitable for weak light–based photochemistry.

In addition to increasing the reaction speed of weak-light reactions, some photochemical experiments require real-time monitoring to precisely understand the internal process, e.g., Raman spectrum and nonlinear optical measurements. For such applications, it is essential to avoid the influences of probe light or lasers. The black TiO_2 metasurfaces can perfectly solve this problem. According to Fig. 1D, the absorption of black TiO_2 is dependent on the ion implantation time. If TiO_2 is implanted with H^+ ions for a very short time, the increased absorption in the visible spectrum is negligibly

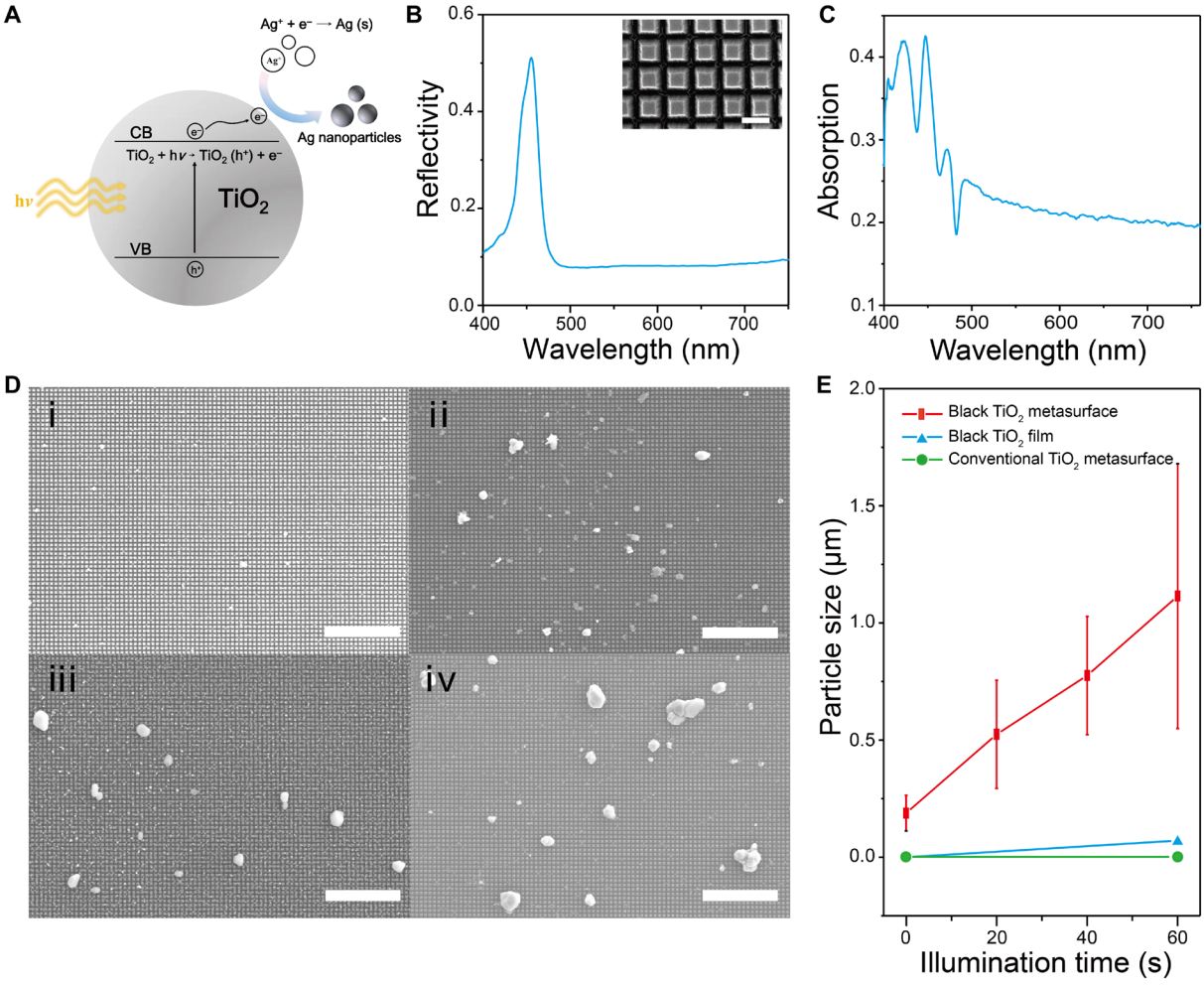

Fig. 4. The black TiO_2 metasurface–based photochemistry. (**A**) Schematic picture of the photoreduction of Ag nanoparticles in solutions. (**B**) Reflection spectrum of the TiO_2 metasurface. The inset is the top-view SEM image. Scale bar, 400 nm. (**C**) Absorption spectrum of the black TiO_2 metasurface. Here, the black TiO_2 was implanted with H^+ ions for 4 min. (**D**) Top row SEM images of the black TiO_2 metasurface after immersing it in $AgNO_3$ solutions for (i) 0 s, (ii) 20 s, (iii) 40 s, and (iv) 60 s. Scale bars, 3 μm (i) and 5 μm (ii, iii, and iv). (**E**) Function of mean particle sizes with different illuminating times of the black TiO_2 metasurface (red square line), the black TiO_2 film (blue triangle line), and the conventional TiO_2 metasurface (green dot line).

small. However, once the TiO_2 film is patterned to the metasurface, the resonance of the metasurface can greatly enhance the absorption around the reflection peak and thus form a narrow absorption band. One example is shown in Fig. 5. A metasurface with lattice size l = 400 nm produced a narrow-band reflection at 630 nm (see the solid line in Fig. 5A). Then, the TiO_2 metasurface was implanted with H^+ ions for a minute. In contrast to the small change of absorption in TiO_2 film, the reflection peak significantly decreased from 50 to 30%, and an obvious absorption peak emerged (see Fig. 5A and fig. S9C).

The slight increase in absorption and the resonant enhancement of incident light (solid line in Fig. 5B) makes the light-implanted TiO_2 metasurface essential for wavelength-dependent photochemistry. To test this application, we have immersed the black TiO_2 metasurface into $AgNO_3$ solution and illuminated it with a tunable laser (see Materials and Methods). Here, the pumping density and time were kept at 10 μJ/cm^2 and 90 s, respectively. The laser wavelengths scanned from 700 to 600 nm. From the corresponding SEM images (fig. S11, B to I), the sizes of Ag nanoparticles have been analyzed and plotted as a function of incident laser wavelength in Fig. 5B. The photochemical reaction was fastest at 640 nm. The sizes of Ag nanoparticles decreased rapidly when the incident wavelength deviated from the resonant peak, giving an FWHM of around 20 nm. Both the peak position and the FWHM matched the retrieved enhancement factor in solution very well. We thus can confirm the importance of the TiO_2 metasurface in wavelength-dependent chemical reactions and chemical processes requiring real-time measurement.

In summary, we have developed a CMOS-compatible technique that can gently and reversibly convert TiO_2 metasurfaces to black TiO_2 metasurfaces without spoiling their internal nanostructures. Consequently, we expanded the practical applications of TiO_2 metasurface from planar visible photonics to photochemistry. By controlling the conversion time, TiO_2 metasurfaces can either accelerate the chemical reaction speed or selectively respond to designed wavelengths. In addition, by-products of active metadevices have also been demonstrated. The research on black TiO_2 metasurfaces shall open new routes to novel photonic devices and even beyond photonics.

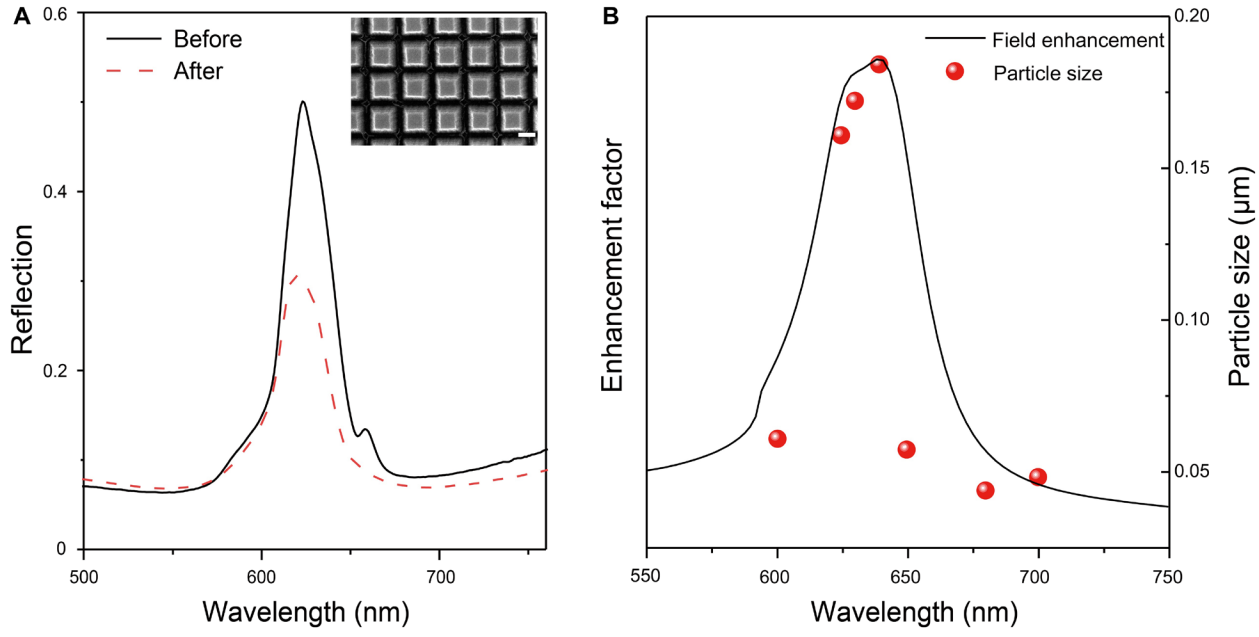

Fig. 5. TiO_2 metasurface–based narrow-band absorber. (**A**) Reflection spectra of the TiO_2 metasurface with $l = 400$ nm before (solid line) and after (dashed line) 1-min H^+ ion implantation. The inset shows the top-view SEM image. Scale bar, 200 nm. (**B**) Enhancement factor (solid line) of light and the sizes (dots) of Ag nanoparticles as a function of wavelength.

MATERIALS AND METHODS

Numerical simulation

The reflection spectra and corresponding field distributions were numerically calculated with a commercial finite element analysis software (COMSOL Multiphysics). In our numerical calculations, the whole structure was composed of TiO_2 and settled on top of a 15-nm ITO-coated glass. The optical constant of TiO_2 was determined from spectroscopic ellipsometry measurements. The dielectric constant of ITO was taken from (*19*). The glass substrate was considered as lossless with a refractive index of $n_{sub} = 1.52$. To mimic the infinite large periodic sample, a periodic boundary condition was applied.

Fabrication of the TiO_2 metasurface

The TiO_2 metasurfaces were fabricated with E-beam lithography, followed by a lift-off process. The ITO glass substrates were cleaned in ultrasound bath in acetone, isopropyl alcohol, and deionized (DI) water for 15 min, respectively, and dried under clean nitrogen flow. Then, 350 nm of ZEP520 film was spin-coated onto the ITO glass substrates and baked at 180°C for 10 min. Afterward, the designed nanostructures were patterned with an electron beam in an E-beam writer (Raith eLINE, 30 kV) and developed in ND510 solution and methyl isobutyl ketone at 0°C for 60 and 10 s, respectively. The samples were transferred into an E-beam evaporator and directionally coated with 200-nm TiO_2 films (deposition rate, 0.8 Å/s; base vacuum pressure, 2×10^{-7} torr). After immersing the samples in acetone for 8 hours, the ZEP patterns were removed and the designed TiO_2 metasurfaces were obtained.

Transition between TiO_2 and black TiO_2

The TiO_2 metasurfaces were transferred to black TiO_2 metasurfaces in an ICP (Oxford Instruments Plasma Technology 380) treatment system. The chamber was pumped to reach a degree of vacuum of around 10^{-9} torr. Then, the metasurfaces were implanted with H^+ plasma with a flow rate of 50 standard cubic centimeters per minute. Meanwhile, the chamber pressure was stabilized at 15 mtorr, and the temperature of the platform was maintained at 70°C. The ICP power was 700 W, and the radio frequency (RF) power was 10 W. Under the same conditions, the black TiO_2 can be oxidized back to TiO_2 by using O^- plasma.

Optical characterization

The sample was placed onto a three-dimensional translation stage under an optical microscope (ZEISS, Axioscope AI). Basically, a collimated white light beam was focused onto a sample by an objective lens (numerical aperture = 0.4). The reflected light (R) was collected and collimated by the same objective lens and coupled to a charge-coupled device (CCD) coupled spectrometer (Acton Research 2750, Princeton Instruments CCD). The transmitted light was collected by another optical lens and coupled to the same spectrometer. The experimental setup of optical characterization is shown in fig. S6A, and the specific method to achieve absorption curve is shown in fig. S6B. The bright-field microscopy images were taken with a Canon EOS 100D camera under the optical microscope.

Photoreduction of Ag nanoparticles

Silver nitrate was prepared as a 0.25 M solution as a silver ion source. First, the sample was immersed in $AgNO_3$ solutions and illuminated with white light or a single-wavelength laser. After illumination, the sample was rinsed with deionized water and then blow-dried with a nitrogen gun. Then, the sizes of the Ag nanoparticles generated on the surface of TiO_2 metasurfaces or films were characterized by SEM. The details and experimental setup are shown in the Supplementary Materials (fig. S9).

SUPPLEMENTARY MATERIALS

Supplementary material for this article is available at http://advances.sciencemag.org/cgi/content/full/5/11/eaax0939/DC1

Supplementary Text

Section S1. The deposition and transition of TiO_2 film

Section S2. Fabrication process and characterization of the nanostructures

Section S3. Numerical calculation and the Mie resonances in TiO_2 metasurfaces

Section S4. Characterization of TiO_2 metasurfaces

Section S5. Dynamic image in TiO_2 metasurfaces

Section S6. The photoreduction with TiO_2 metasurfaces

Fig. S1. The deposition and transition of TiO_2 film.

Fig. S2. Fabrication process and characterization of the nanostructures.

Fig. S3. Numerical calculation and the Mie resonances in TiO_2 metasurfaces.

Fig. S4. The numerical simulation of Mie resonance.

Fig. S5. The numerical simulation of the TiO_2 metasurface before and after H^+ implantation.

Fig. S6. Optical measurement of TiO_2 metasurfaces.

Fig. S7. The color and reflection spectrum of TiO_2 metasurfaces.

Fig. S8. The SEM image of "COLOR" pattern without guide lines.

Fig. S9. Setup for photoreduction and the characterization of the TiO_2 metasurface in $AgNO_3$ solution.

Fig. S10. The contrast experiment of Ag photoreduction and characterization of the generated Ag nanoparticle.

Fig. S11. Characterization of particle sizes of Ag photoreduction on TiO_2 metasurfaces.

REFERENCES AND NOTES

1. N. Yu, P. Genevet, M. A. Kats, F. Aieta, J.-P. Tetienne, F. Capasso, Z. Gaburro, Light propagation with phase discontinuities: Generalized laws of reflection and refraction. *Science* **334**, 333–337 (2011).
2. X. Ni, N. K. Emani, A. V. Kildishev, A. Boltasseva, V. M. Shalaev, Broadband light bending with plasmonic nanoantennas. *Science* **335**, 427 (2012).
3. N. Yu, F. Capasso, Flat optics with designer metasurfaces. *Nat. Mater.* **13**, 139–150 (2014).
4. A. V. Kildishev, A. Boltasseva, V. M. Shalaev, Planar photonics with metasurfaces. *Science* **339**, 1232009 (2013).
5. D. Lin, P. Fan, E. Hasman, M. Brongersma, Dielectric gradient metasurface optical elements. *Science* **345**, 298–302 (2014).
6. X. Ni, A. V. Kildishev, V. M. Shalaev, Metasurface holograms for visible light. *Nat. Commun.* **4**, 2807 (2013).
7. B. Wang, F. Dong, Q.-T. Li, D. Yang, C. Sun, J. Chen, Z. Song, L. Xu, W. Chu, Y.-F. Xiao, Q. Gong, Y. Li, Visible-frequency dielectric metasurfaces for multiwavelength achromatic and highly dispersive holograms. *Nano Lett.* **16**, 5235–5240 (2016).
8. A. Kristensen, J. K. W. Yang, S. I. Bozhevolnyi, S. Link, P. Nordlander, N. J. Halas, N. A. Mortensen, Plasmonic colour generation. *Nat. Rev. Mater.* **2**, 16088 (2017).
9. W. T. Chen, K.-Y. Yang, C.-M. Wang, Y.-W. Huang, G. Sun, I.-D. Chiang, C. Y. Liao, W.-L. Hsu, H. T. Lin, S. Sun, L. Zhou, A. Q. Liu, D. P. Tsai, High-efficiency broadband meta-hologram with polarization-controlled dual images. *Nano Lett.* **14**, 225–230 (2014).
10. Y. Fu, A. Kuznetsov, A. Miroshnichenko, Y. Yu, B. Luk'yanchuk, Directional visible light scattering by silicon nanoparticles. *Nat. Commun.* **4**, 1527 (2013).
11. M. Khorasaninejad, W. T. Chen, R. C. Devlin, J. Oh, A. Y. Zhu, F. Capasso, Metalenses at visible wavelengths: Diffraction-limited focusing and subwavelength resolution imaging. *Science* **352**, 1190–1194 (2016).
12. R. C. Devlin, M. Khorasaninejad, W. T. Chen, J. Oh, F. Capasso, Broadband high-efficiency dielectric metasurfaces for the visible spectrum. *Proc. Natl. Acad. Sci. U.S.A.* **113**, 10473–10478 (2016).
13. S. Sun, Z. Zhou, C. Zhang, Y. Gao, Z. Duan, S. Xiao, Q. Song, All-dielectric full-color printing with TiO_2 metasurfaces. *ACS Nano* **11**, 4445–4452 (2017).
14. R. C. Devlin, A. Ambrosio, N. Rubin, J. Mueller, F. Capasso, Arbitrary spin-to-orbital angular momentum conversion of light. *Science* **358**, 896–901 (2017).
15. Z. Shi, M. Khorasaninejad, Y.-W. Huang, C. Roques-Carmes, A. Y. Zhu, W. T. Chen, V. Sanjeev, Z.-W. Ding, M. Tamagnone, K. Chaudhary, R. C. Devlin, C.-W. Qiu, F. Capasso, Single-layer metasurface with controllable multiwavelength functions. *Nano Lett.* **18**, 2420–2427 (2018).
16. W. T. Chen, A. Y. Zhu, V. Sanjeev, M. Khorasaninejad, Z. Shi, E. Lee, F. Capasso, A broadband achromatic metalens for focusing and imaging in the visible. *Nat. Nanotechnol.* **13**, 220–226 (2018).
17. S. Wang, P. C. Wu, V.-C. Su, Y.-C. Lai, M.-K. Chen, H. Y. Kuo, B. H. Chen, Y. H. Chen, T.-T. Huang, J.-H. Wang, R.-M. Lin, C.-H. Kuan, T. Li, Z. Wang, S. Zhu, D. P. Tsai, A broadband achromatic metalens in the visible. *Nat. Nanotechnol.* **13**, 227–232 (2018).
18. W. T. Chen, A. Y. Zhu, J. Sisler, Y.-W. Huang, K. M. A. Yousef, E. Lee, C.-W. Qiu, F. Capasso, Broadband achromatic metasurface-refractive optics. *Nano Lett.* **18**, 7801–7808 (2018).
19. W. T. Chen, A. Y. Zhu, J. Sisler, Z. Bharwani, F. Capasso, A broadband achromatic polarization-insensitive metalens consisting of anisotropic nanostructures. *Nat. Commun.* **10**, 355 (2019).
20. M. Henstridge, C. Pfeiffer, D. Wang, A. Boltasseva, V. M. Shalaev, A. Grbic, R. Merlin, Synchrotron radiation from an accelerating light pulse. *Science* **362**, 439–442 (2018).
21. H. Pahlevaninezhad, M. Khorasaninejad, Y.-W. Huang, Z. Shi, L. P. Hariri, D. C. Adams, V. Ding, A. Zhu, C.-W. Qiu, F. Capasso, M. J. Suter, Nano-optic endoscope for high-resolution optical coherence tomography in vivo. *Nat. Photonics* **12**, 540–547 (2018).
22. A. Fujishima, X. Zhang, D. Tryk, TiO_2 photocatalysis and related surface phenomena. *Surf. Sci. Rep.* **63**, 515–582 (2008).
23. X. Chen, L. Liu, Y. Peter, S. Mao, Increasing solar absorption for photocatalysis with black hydrogenated titanium dioxide nanocrystals. *Science* **331**, 746–750 (2011).
24. X. Chen, L. Liu, F. Huang, Black titanium dioxide (TiO_2) nanomaterials. *Chem. Soc. Rev.* **44**, 1861–1885 (2015).
25. N. Liu, V. Häublein, X. Zhou, U. Venkatesan, M. Hartmann, M. Mačković, T. Nakajima, E. Spiecker, A. Osvet, L. Frey, P. Schmuki, "Black" TiO_2 nanotubes formed by high-energy proton implantation show noble-metal-co-catalyst free photocatalytic H_2-evolution. *Nano Lett.* **15**, 6815–6820 (2015).
26. N. Liu, C. Schneider, D. Freitag, M. Hartmann, U. Venkatesan, J. Müller, E. Spiecker, P. Schmuki, Black TiO_2 nanotubes: Cocatalyst-free open-circuit hydrogen generation. *Nano Lett.* **14**, 3309–3313 (2014).
27. Z. Wu, Z.-K. Zhang, D.-Z. Guo, Y.-J. Xing, G.-M. Zhang, Titanium oxide nanospheres: Preparation, characterization, and wide-spectral absorption. *Phys. Status Solidi A Appl. Mater. Sci.* **209**, 2020–2026 (2012).
28. B. Bharti, S. Kumar, H.-N. Lee, R. Kumar, Formation of oxygen vacancies and Ti^{3+} state in TiO_2 thin film and enhanced optical properties by air plasma treatment. *Sci. Rep.* **6**, 32355 (2016).
29. Q. Song, S. Xiao, Z. Xu, J. Liu, X. Sun, V. Drachev, V. M. Shalaev, O. Akkus, Y. L. Kim, Random lasing in bone tissue. *Opt. Lett.* **35**, 1425–1427 (2010).
30. S. Sun, W. Yang, C. Zhang, J. Jing, Y. Gao, X. Yu, Q. Song, S. Xiao, Real-time tunable colors from microfluidic reconfigurable all-dielectric metasurfaces. *ACS Nano* **12**, 2151–2159 (2018).
31. J. Li, S. Kamin, G. Zheng, F. Neubrech, S. Zhang, N. Liu, Addressable metasurfaces for dynamic holography and optical information encryption. *Sci. Adv.* **4**, eaar6768 (2018).
32. X. Duan, S. Kamin, N. Liu, Dynamic plasmonic colour display. *Nat. Commun.* **8**, 14606 (2017).
33. L. Zhou, D. F. Swearer, C. Zhang, H. Robatjazi, H. Zhao, L. Henderson, L. Dong, P. Christopher, E. A. Carter, P. Nordlander, N. J. Halas, Quantifying hot carrier and thermal contributions in plasmonic photocatalysis. *Science* **362**, 69–72 (2018).
34. J. Yang, Y. Guo, R. Jiang, F. Qin, H. Zhang, W. Lu, J. Wang, J. C. Yu, High-efficiency "Working-in-tandem" nitrogen photofixation achieved by assembling plasmonic gold nanocrystals on ultrathin titania nanosheets. *J. Am. Chem. Soc.* **140**, 8497–8508 (2018).
35. Y. G. Sun, Y. N. Xia, Shape-controlled synthesis of gold and silver nanoparticles. *Science* **298**, 2176–2179 (2002).
36. X. M. Goh, Y. Zheng, S. J. Tan, L. Zhang, K. Kumar, C.-W. Qiu, J. K. W. Yang, Three-dimensional plasmonic stereoscopic prints in full colour. *Nat. Commun.* **5**, 5361 (2014).
37. X. Pan, Y.-J. Xu, Fast and spontaneous reduction of gold ions over oxygen-vacancy-rich TiO_2: A novel strategy to design defect-based composite photocatalyst. *Appl. Catal. A* **459**, 34–40 (2013).

Acknowledgments: We acknowledge valuable discussions with J. Han and H. Ji. **Funding:** This research was supported by the National Key Research and Development Project (grant no. 2018YFB2200403) and Shenzhen Fundamental research projects under grant no. JCYJ20180507184613841. We thank the support from the Shenzhen Engineering Laboratory on organic-inorganic perovskite devices. **Author contributions:** Y.W. and W.Y. designed and fabricated the metasurfaces. Y.W. and Y.F. measured the optical properties of TiO_2 metasurfaces. Y.W. implemented the photochemistry experiment. Q.S. and S.X. supervised the project and wrote the manuscript. **Competing interests:** The authors declare that they have no competing interests. **Data and materials availability:** All data needed to evaluate the conclusions in the paper are present in the paper and/or the Supplementary Materials. Additional data related to this paper may be requested from the authors.

Submitted 21 February 2019
Accepted 17 September 2019
Published 1 November 2019
10.1126/sciadv.aax0939

Citation: Y. Wu, W. Yang, Y. Fan, Q. Song, S. Xiao, TiO_2 metasurfaces: From visible planar photonics to photochemistry. *Sci. Adv.* **5**, eaax0939 (2019).